J. Plasma Phys. (2024), *vol*. 90, 975900501
Published by Cambridge University Press
doi:10.1017/S0022377824000813

Experimental study on the formation and evolution of unconfined counter-helicity spheromaks merging using magnetized coaxial plasma gun

Liangwen Qi [1,2,†], **Jian Song** [2], **Fantao Zhao** [2], **Siqi Yu** [3], **Chongxiao Zhao** [4], **Huijie Yan** [2] **and Dezhen Wang** [2]

[1]School of Mathematics and Physics, Lanzhou Jiaotong University, Lanzhou 730070, Gansu, PR China

[2]Key Laboratory of Materials Modification by Laser, Ion and Electron Beams (Ministry of Education), School of Physics, Dalian University of Technology, Dalian 116024, PR China

[3]Department of Physik und Astronomie, Ruhr-University Bochum, Bochum, D-44780, Germany

[4]State Key Laboratory of Laser Interaction with Matter, Changchun Institute of Optics, Fine Mechanics and Physics, Chinese Academy of Sciences, Changchun 130033, PR China

(Received 3 September 2023; revised 26 June 2024; accepted 1 July 2024)

The formation and evolution of unconfined counter-helicity spheromaks merging have been experimentally investigated by using a magnetized coaxial plasma gun. By comparing the time-dependent photodiode signals and plasma radiation images of counter-helicity spheromaks merging and plasma jets merging, it is found that the field-reversed configuration (FRC) plasma formed by counter-helicity spheromaks merging has a distinct contour and a long maintenance time. For plasma jets merging, the resulting plasma has no discernible contours and a shorter lifetime. In addition, it is inferred from these data that stagnation heating and magnetic reconnection events occur during the counter-helicity spheromaks merging, causing a rapid rise in plasma pressure at the merging midplane and sharp kinks in the field lines near the merger region. By changing different operating parameters and observing the impact on the merger characteristics, it is suggested that the qualitative dynamics of the FRC plasma depends on the balance between the plasma pressure and the magnetic pressure. The high discharge voltage breaks the equilibrium in the merged body, while the large gas-puffed mass just weakens the compression effect of the merged body. These results give us an intuitive understanding of the counter-helicity spheromak merger process and its dependence on discharge parameters, and also provide a distinct perspective for the optimal design of FRC.

Keywords: coaxial gun, spheromak, plasma jet, collisional merging, field-reversed configuration

† Email address for correspondence: 18742509171@163.com

1. Introduction

Spheromaks (Jarboe 1994, 2005) and field-reversed configurations (FRCs) (Steinhauer 2011) belong to the compact torus (Furth 1981) subclass of magnetic fusion configurations. The magnetic field in spheromaks has toroidal and poloidal components of similar magnitude, while the magnetic field in FRC is purely poloidal. Both configurations act as multi-energy self-organized carriers with kinetic energy (accelerated), thermal energy and electromagnetic energy, and must rely on internal plasma currents to maintain their individual magnetic topologies. The difference is that the plasma current in a spheromak is dominantly parallel to the magnetic field, while the plasma current in an FRC is primarily perpendicular to the field. These plasmas have been studied for many reasons motivated by their broad range of applications, such as a refuelling scheme for fusion machines (Parks 1988; Brown & Bellan 1992; Nagata *et al.* 2005; Matsumoto *et al.* 2016), studies of magnetic field reconnection and instabilities in plasmas (Yamada *et al.* 1990; Ono, Yamada & Akao 1996; Geddes, Kornack & Brown 1998; Kornack, Sollins & Brown 1998; Hsu & Bellan 2005; Gray *et al.* 2010), as a magnetized target for magneto-inertial fusion (Stanic, Cassibry & Adams 2013; Vyas & Cassibry 2020; Byvank *et al.* 2021) and in basic science studies of highly self-organized plasmas (Janos *et al.* 1985; Ono *et al.* 1999; Kawamori & Ono 2005).

The FRC is a plasmoid that is particularly appealing for containing thermonuclear plasmas due to its high β value (ratio of plasma pressure to magnetic pressure), simply connected magnetic structure and easy transferability. The FRC has been produced by various methods such as rotating magnetic fields (Hoffman *et al.* 2006), theta-pinch formation (Steinhauer 2011), coaxial slow source (Pietrzyk *et al.* 1987; Pierce *et al.* 1993) and merging spheromaks with opposite helicities (Ono *et al.* 1999; Cothran *et al.* 2003; Gerhardt *et al.* 2008; Horiuchi, Moritaka & Usami 2018). As one of the FRC creation methods, counter-helicity spheromaks merging is used to obtain an FRC with no or little toroidal magnetic field by merging two spheromaks with opposite toroidal magnetic fields. In this process, two spheromaks in close proximity combine via magnetic reconnection and eventually relax to a lower-energy state. A spheromak is typically formed by a magnetized coaxial plasma gun. Initially, a slowly rising radial magnetic field is imposed in the gun region by internal-bias solenoid coils. Neutral gas is then injected by fast gas-puff valves prior to applying a high voltage to the electrodes. After gas breakdown, radial current $\boldsymbol{J}$ is generated between the inner and outer electrodes, the azimuth magnetic field $\boldsymbol{B}$ is generated by the current flowing through the inner electrode and the resultant $\boldsymbol{J} \times \boldsymbol{B}$ force pushes the plasma forward. For the appropriate current threshold of spheromak formation, once the force exceeds the tension of the bias field, the field lines will be stretched, torn and eventually reconnected to form a spheromak ejection. A spheromak with opposite helicity is achieved by changing the direction of the solenoid current while keeping the polarity of the gun power supply.

The formation and equilibrium of FRCs produced by counter-helicity spheromaks merging have been investigated both theoretically and experimentally (Lukin *et al.* 2001; Cothran *et al.* 2003; Kawamori & Ono 2005; Kaminou *et al.* 2017; Nishida, Horiuchi & Ono 2019). Co-helicity and counter-helicity spheromak merging experiments were first started by Yamada *et al.* (1990) at the University of Tokyo in 1990 to study the magnetic reconnection phenomenon. The results show that the direction of the toroidal magnetic field plays an important role in the merger process, and the merger of the counter-helicity is much faster than that of the co-helicity spheromak. In addition, the magnetic reconnection rate is proportional to the initial relative velocities of the two spheromaks, indicating that the magnetic reconnection is a forced phenomenon. The Swarthmore Spheromak

https://doi.org/10.1017/S0022377824000813 Published online by Cambridge University Press

Experiment (SSX) has been devoted to studying the basic physics of spheromak formation and using stable spheromaks as force-free reservoirs of magnetic flux for merging and magnetic reconnection experiments. It involves magnetic reconnection events (Brown *et al.* 2006), strong ion flow effects (Brown *et al.* 2002), Taylor relaxation processes and the generation and development of instability (Belova *et al.* 2006; Cothran *et al.* 2010). Furthermore, Cothran et al. (2003) optimized the SSX configuration by designing a pair of coils in the midplane to restrict the merger process, and determined the dependence of the stability of the final magnetic structure on the quantity of toroidal flux remaining from the initial spheromaks.

Based on the above analysis, although the formation mechanism and instability control of counter-helicity spheromaks merging have been extensively studied in previous works, all of them have been carried out under the conditions of small-scale flux conservers or the application of poloidal confinement magnetic fields in the midplane. It is inevitable that the flux conserver boundary has an impact on the magnetic field topology, which leaves a lack of intuitive information on a comprehensive understanding of the counter-helicity spheromak merger process, especially in terms of evolutionary details. Furthermore, the presence or absence of a poloidal field is the main reason for affecting the lifetime of the plasma merged body. Unlike the spheromak, which is injected into the poloidal magnetic field during the production process, the plasma jet is only embedded in the toroidal magnetic field structure due of the 'frozen-in-field-line' effects. The velocity and density of the entire plasma jet are higher, while the temperature is lower. Thus, one of the objectives of this paper is to compare the formation and evolution characteristics of unconfined plasma jets merging and counter-helicity spheromaks merging.

In addition to the change of magnetic field characteristics, the accompanying energy conversion in the counter-helicity spheromak merger process has also attracted attention. The advantage of counter-helicity spheromaks merging to form FRC is that a large poloidal flux can be obtained during the slow formation process, and the total helicity of the system is zero. As one of the heating sources during the merger process, magnetic reconnection converts magnetic energy into plasma thermal energy much faster than Joule heating. Previous simulations and experiments (Yoo *et al.* 2013; Yamada *et al.* 2014) have found that there is a Hall electric field around the reconnection X point, which contributes to the generation of flow and energy conversion. Horiuchi *et al.* (2018) and Makwana, Keppens & Lapenta (2018) simulated the co-helicity and counter-helicity spheromak merger processes, and the results showed that the ion temperature peaks due to the meandering motion of ions during the counter-helicity merger process, while the ion temperature tends to be flat or hollow during the co-helicity merger process. Similar to the counter-helicity spheromaks merging, Kobayashi *et al.* (2021) performed the collisional merging formation of an FRC in the FAT-CM (FRC amplification via translation-collisional merging) device, and the results showed that shockwaves are excited via collision of two accelerated plasmas and that the excited shock causes energy regeneration of kinetic energy back into thermal plasma energy. However, as a carrier of energy, little is known about the dependence of counter-helicity spheromaks merging on plasma parameters. Therefore, another goal of this paper is to analyse the dynamics of FRC formation and give the basis for discharge parameter optimization.

In this paper, based on the formation of magnetized target in a magneto-inertial fusion scheme, a spheromak merging device with magnetized coaxial gun as the plasma source is constructed to investigate the formation, evolution and equilibrium characteristics of the FRC. The discharge images, electrical characteristics and light emission signals of the plasma collision are acquired. The characteristics of counter-helicity spheromaks merging and plasma jets merging under the same discharge parameters are compared, which further

https://doi.org/10.1017/S0022377824000813 Published online by Cambridge University Press

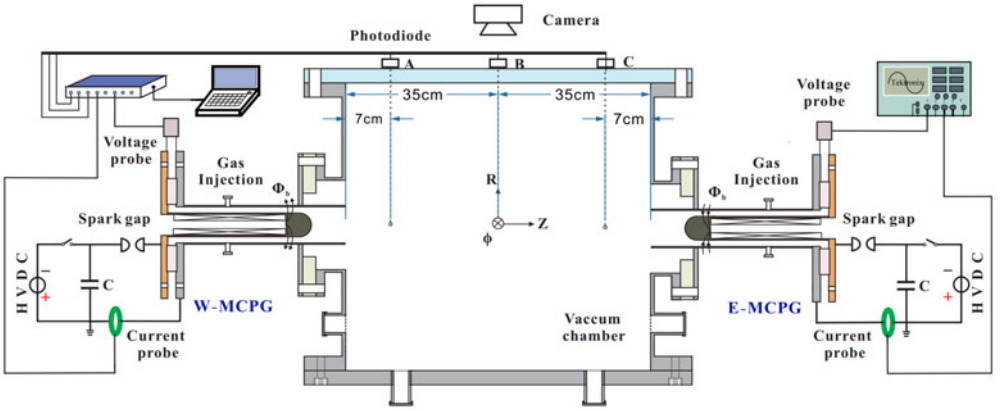

FIGURE 1. Schematic of the whole experimental set-up.

confirms the confinement effect of the poloidal magnetic field on the plasma in the FRC. In addition, by changing different discharge parameters (discharge voltage, gas-puffed mass), the fundamental physical mechanism of its effect on the merging equilibrium of the counter-helicity spheromaks merging is discussed.

2. Experimental set-up and diagnostics

2.1. *The experimental set-up*

A schematic diagram of the whole experimental set-up is shown in figure 1, consisting mainly of two capacitive energy storage systems, two coaxial plasma guns, four gas-puff valves, two bias coils and a vacuum system. The two magnetized coaxial plasma gun systems used in the present experiment have exactly the same configuration and specifications, and the detailed configuration parameters have been described in a previous paper (Qi *et al.* 2020, 2021). In order to reflect the experimental device more directly, the overall design drawing in figure 2 is given. The inner electrode (cathode) is a 343 mm long, 54 mm outer diameter hollow copper tube with a welded hemispherical W-Cu alloy head. The outer electrode (anode) is a 388 mm long, 83.1 mm inner diameter stainless-steel tube. The thicknesses of these electrodes are 3 mm. The gun is powered by a 150 μF spark-switched capacitor bank which operates in a range of 11–15 kV charge voltage with a negative polarity. The fixed bias magnetic flux Φ_b is 2.7 mWb, which is provided by a solenoid coil installed inside the inner electrode. The antiparallel helicity of the spheromak is achieved by changing the current direction in the solenoid. For each gun, two gas-puff valves are tangentially arranged on the outer electrode to enable that neutral gas diffuses uniformly in the azimuthal direction. The two coaxial plasma guns are mounted oppositely on the end wall of a cylindrical vacuum chamber with a diameter of 700 mm and height of 666 mm through an insulating flange. The top of the chamber was covered with tempered glass providing generous optical access to view the evolution of the plasma dynamics. The large size of the chamber effectively avoids plasma–wall interactions and eliminates the impact of flux conserver boundary on the magnetic field topology. The vacuum is maintained by a turbo molecular pump, providing a $\sim 10^{-3}$ Pa background pressure. Pure argon is puffed into the inter-electrode space for plasma generation. The puffed gas mass can be adjusted by changing the amplitude of the pulsed current via electromagnetic valve supplies.

https://doi.org/10.1017/S0022377824000813 Published online by Cambridge University Press

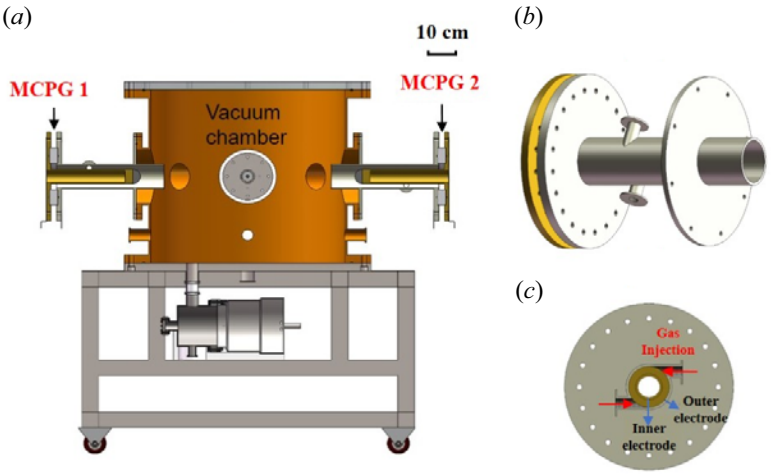

FIGURE 2. Design of the (*a*) overall experimental devices, (*b*) magnetized coaxial gun structure and (*c*) gun structure cross-section.

2.2. *Diagnostics*

The geometry of the experiment is characterized by a cylindrical coordinate system (r, φ, z), where z is the direction along the axis of symmetry, φ is the azimuthal direction about the axis and r is the radial distance from the axis. All diagnostics used in the experiment are also shown in figure 1. For each gun, the discharge current is measured by a Pearson 1423 current probe, and the voltage between two electrodes is measured by a differential probe. To display the morphologic characteristics of plasma ejection merging, two of the three photodiodes (Thorlabs PDA-10A, 200–1100 nm, 150 MHz) are placed at 7 cm from the muzzle of the gun. The remaining one is arranged 35 cm from the muzzle, looking at the chamber centre near the merger region. The plasma optical signal perpendicular to the Z-axis propagation direction is collected through transparent tempered glass. The parallel light is collected by the collimation lens (Thorlabs F240SMA-A) and enters the photodiodes through an optical fibre. Once the plasma propagates to the position where the collimator is placed, the photodiode outputs a voltage signal of a certain amplitude. This signal is positively correlated with the luminous intensity of the plasma. Those signals from the current probes, differential probes and photodiodes are recorded on synchronously triggered a four-channel oscilloscope (Tektronix DPO4104B) and eight-channel oscilloscope (PicoScope 4828). The macroscopic plasma radiation colour images from the top view are captured by a digital camera (Nikon D7000) with an exposure time of 1 s. The collected light is in the continuum visible range. In addition, in order to observe the evolution of counter-helicity spheromak formation and merging, a high-speed camera (Phantom VEO 410L) is placed on top of the chamber to capture its images.

2.3. *Discharge operation sequence*

The discharge time sequence of two magnetized coaxial plasma guns is shown in figure 3. The operation sequence of plasma formation in the experiment must be synchronized. All timing trigger signals are provided by a time-adjustable fibre coupling delay trigger system. The operation sequence of a typical spheromak discharge proceeds as follows: initially, the bias magnetic field power supply is triggered to generate a magnetic field through the solenoid coils embedded in the inner electrode. The corresponding peak

https://doi.org/10.1017/S0022377824000813 Published online by Cambridge University Press

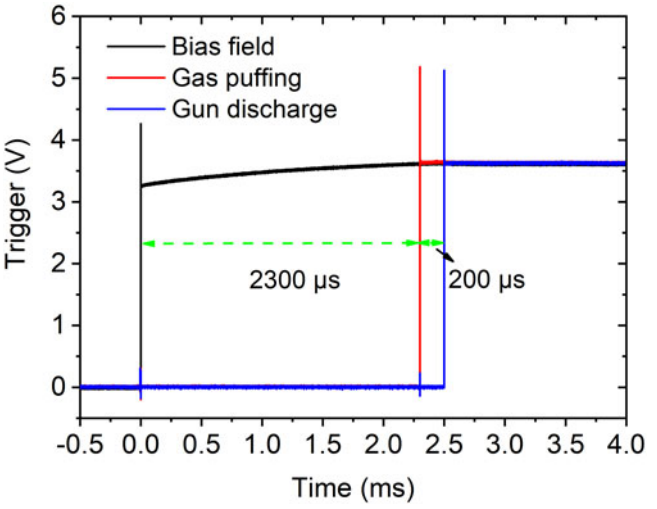

FIGURE 3. Operation sequence of magnetized coaxial plasma gun discharge.

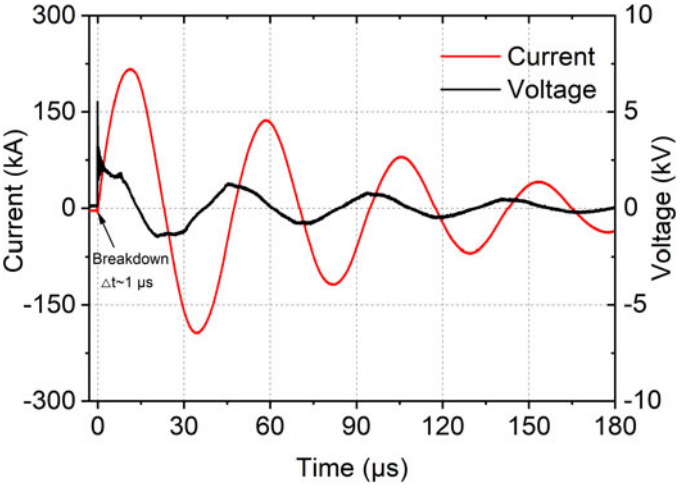

FIGURE 4. Traces of gun current and voltage between two electrodes for a typical plasma shot.

current is 1 kA, bias flux is 2.7 mWb and the magnetic field is divergently distributed on the end face of the solenoid. Then two gas-puff valves are triggered 2.3 ms after the bias flux bank. Lastly, the main gun capacitor bank is fired 200 μs afterward. Simultaneously, the digitization of various diagnostic waveforms is initiated and the high-speed camera is triggered. It is important to note that the driving current duration of the bias magnetic field is approximately 10 ms and the rise time is 2.5 ms. The long pulse not only ensures that its bias magnetic field penetrates the inner electrode wall to the discharge gap, but also ensures that the magnetic field is essentially stationary on the pulse time scale of the coaxial gun discharge (~23.5 μs). In plasma jet experiments, the voltage of the bias magnetic field power supply is adjusted to zero so that the magnetic flux is zero.

By triggering the spark switch connected to the capacitor bank, a high voltage is applied to the electrodes, after which the gas breaks down and a plasma is generated in the gun. Typical current and voltage waveforms are displayed in figure 4. The time interval

https://doi.org/10.1017/S0022377824000813 Published online by Cambridge University Press

from triggering the spark switch to gas breakdown is approximately 1 μs, which has a negligible effect on the whole delay adjustment. After gas breakdown, the current flowing through the plasma connects the inner and outer electrodes to form an *RLC* circuit. The plasma behaves as a primarily reactive load during the discharge, so the circuit exhibits the characteristics of under-damped oscillations. Also, it is noted that the traces are not in phase, implying that the plasma is inductive. Although shots with identical gun parameters generated qualitatively similar waveforms and data, characteristics such as magnitudes and time offsets were often inconsistent. Therefore, we conducted 3–5 shots under each experimental condition, and used the voltage and current waveform as a reference to ensure the consistency of the results.

3. Results and discussion

3.1. *Formation and evolution of counter-helicity spheromaks merging*

For a capacitor charge voltage of 13 kV and a gas-puffed mass of 0.46 mg, oscillograms of the magnetized coaxial gun discharge current signals and photodiode signals of the counter-helicity spheromaks merging are displayed in figure 5. The current amplitude and pulse width are approximately 218 kA and 23.5 μs, respectively, and the difference between the two guns is negligible. The high-frequency components around $t = 0$ appear to be correlated with measuring the photodiode signal (PMT) and gun current simultaneously. Figures 5(*a*) and 5(*b*) show the ejection characteristics of spheromaks with opposite helicity. The photodiode signals indicate that only one spheromak is ejected during the first half-period of current. In the rest of the discharge process, the small secondary feature in figure 5(*a*) may be a small crowbar causing a secondary plasma ejection. Typical characteristics of spheromak plasmas at a distance of 12 cm from the nozzle are equal magnetic fields ($B_z \sim B_\varphi \sim 0.1$ T), 3×10^{15}/cm^3 electron density, 12 eV electron temperature and 70 km s^{-1} velocity (see, in Qi *et al.* 2021). Figure 5(*c*) shows the merger characteristics of the counter-helicity spheromak. It can be seen that the light intensity of the photodiode signal is enhanced after the counter-helicity spheromaks merge, and is stronger than that of any single spheromak. The plasma can be maintained at around 15 μs starting from the moment when the merged photodiode signal appears. During this time, the merged PMT-C waveform between 10 and 20 μs is very similar in shape to that of the plasma source PMT-B waveform between 15 and 22 μs, suggesting that a component of the PMT-C signal corresponds to a spatio-temporal translation of the PMT-B signal. However, there may also be a distinct depression at the peak 24 μs of the PMT-C signal that might be caused by two energy conversion mechanisms described below: (1) the velocity of the high-speed spheromaks drops to zero instantaneously when merging, and the axial kinetic energy of the plasma is converted into heat energy. (2) The magnetic reconnection event accompanying the merger process annihilates the initial spheromak helicities, and the consumed magnetic energy is rapidly converted to electron and ion heat, as well as plasma flow. As a result, the number of high-energy charged particles increases, the recombination between particles decreases, and there may be ultraviolet or even X-ray radiation, which is beyond the collection wavelength range of the photodiode.

In order to obtain visual information on the general structure of the plasma, the exposure time of the camera is adjusted to 1 s, which is longer than the entire discharge period. The time-integrated radiation image of the counter-helicity spheromaks merging recorded by the camera is shown in figure 6. One can see that the spheromaks merge to form an oblate (more spherical) FRC plasma with a radial dimension (∼30 cm) approximately twice the axial dimension (∼15 cm), which is consistent with the typical characteristics of

https://doi.org/10.1017/S0022377824000813 Published online by Cambridge University Press

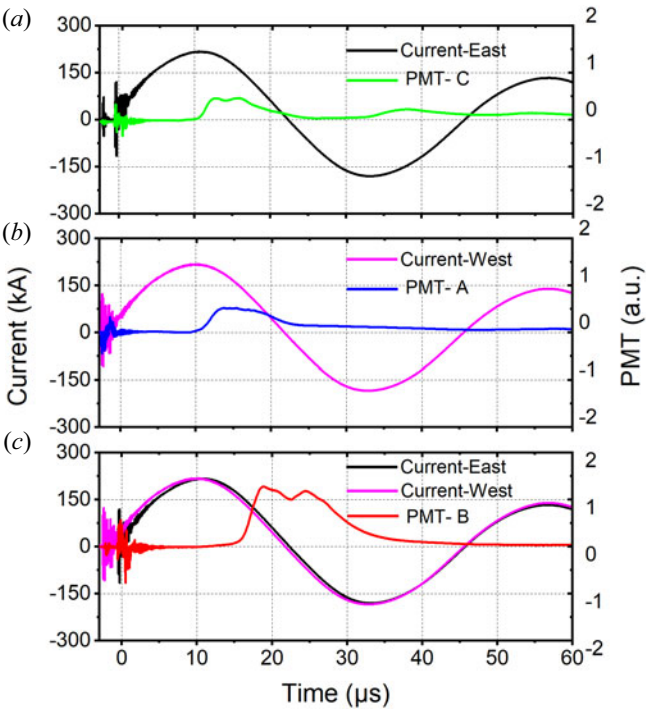

FIGURE 5. Oscillograms of the discharge current and three photodiode signals (PMT-C and A are placed 7 cm from the muzzle, and PMT-B is placed 35 cm from the muzzle) in the counter-helicity spheromak merging experiment, when the capacitor bank charged to 13 kV and the mass of argon puffed is 0.46 mg.

spheromaks merging. For a single spheromak, estimated by its velocity and the full width at half-maximum of the photodiode signal, it is similar to a cylinder with an axial length of 34 cm and a diameter of 15 cm before collision. The resulting FRC plasma is compressed in the axial direction and expands along the radial direction. Another feature we can see is that there is a bright curved surface in the midplane of the merging body, accompanied by some twisted bright filaments. This is due to the fact that the plasma is compressed and heated throughout the merger process, which eventually causes a rise in plasma pressure at the merging midplane, and its light intensity is enhanced. In addition, the appearance of kink features suggests that the magnetic topology of the counter-helicity spheromaks merger is broken (Yamada *et al.* 1990), and field lines with a sharp kink near the merger region guide plasma flow.

In addition to the plasma macro picture presented earlier, a high-speed camera is used to capture the evolution images of the counter-helicity spheromaks merging, as shown in figure 7. The exposure time is 2.66 μs and the interframe time is 9.09 μs. The moment of gas breakdown is taken as the zero-time trigger of the camera. In the initial stage, the plasma breakdown and acceleration occur in the gun, and then the spheromak ejects from the muzzle at 9.09 μs. Finally, the formation, equilibrium and dissipation of the FRC plasma occur during the period of 18.18 $\sim$ 27.27 μs. Upon merging, assuming that the reconnection event annihilates the initial spheromak helicities, the merged plasma will undergo an energy relaxation process consistent with the maintenance time of the photodiode signal. The plasma morphology changes from spherical to convex until it

https://doi.org/10.1017/S0022377824000813 Published online by Cambridge University Press

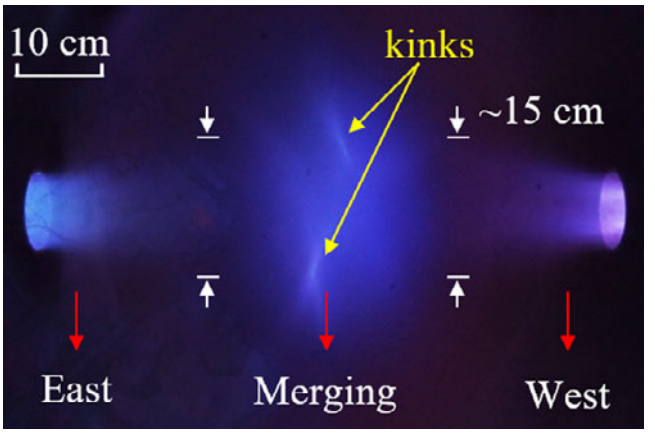

FIGURE 6. Radiation image of the counter-helicity spheromaks merging for a 13 kV shot and an exposure of 1 s. View perpendicular to the gun axis.

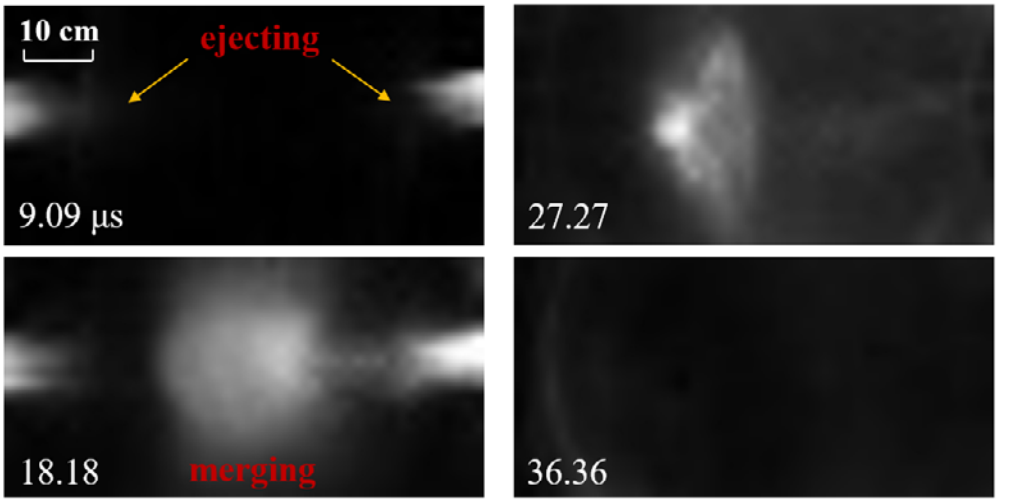

FIGURE 7. Corresponding evolution images of counter-helicity spheromaks merging, and the exposure time is 2.66 μs. View perpendicular to the gun axis.

dissipates completely, which lasts for approximately $10 \sim 15$ μs. It is worth noting that this experiment is based on the unconfined spheromaks merger to study the formation of FRC plasma. Compared with the structure with an external poloidal field in the midplane, the unconfined FRC plasma is confined only by its poloidal magnetic field and the confinement time is relatively short. This dissipation mechanism may be due to the dominance of the $n = 1$ toroidal mode in the late evolution stage, and is consistent with the tilt instability (Cothran *et al.* 2003). As a result, the oblate (radial) FRC plasma tilts rapidly, distorting the magnetic field structure and dissipating the plasma.

3.2. *Two plasma jets merging*

As a comparison and verification, a collision experiment of two plasma jets is carried out. Adjusting the bias magnetic flux to zero, oscillograms of the coaxial gun discharge current signals and photodiode signals of the two plasma jets merging under 13 kV capacitor

https://doi.org/10.1017/S0022377824000813 Published online by Cambridge University Press

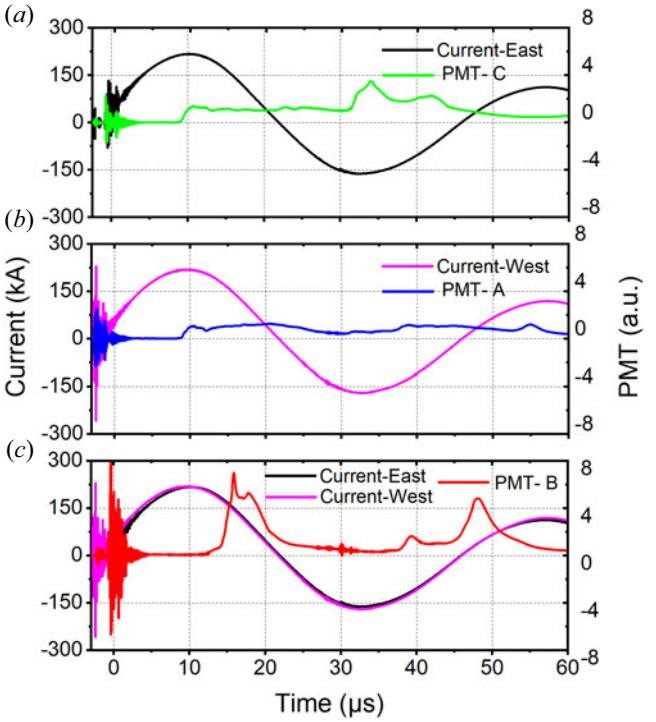

FIGURE 8. Oscillograms of the discharge current and three photodiode signals (PMT-C and A are placed 7 cm from the muzzle, and PMT-B is placed 35 cm from the muzzle) in a two plasma jet merging experiment, when the capacitor bank charged to 13 kV and the mass of argon puffed is 0.46 mg.

charging voltage and 0.46 mg puffed gas are displayed in figure 8. The current amplitude and pulse width are the same as in the case of the magnetized coaxial gun, which implies that the bias magnetic field has little effect on the plasma impedance. The impedance of the total discharge circuit is still dominated by the linear impedance of the outer circuit, and the oscillation characteristics of the circuit hardly change with the change of the bias magnetic field. Figures 8(*a*) and 8(*b*) show the ejection characteristics of the two plasma jets. The photodiode signals show that plasma is also ejected during the remaining discharge cycle in addition to the first half-cycle of the current. Typical characteristics of plasma jets at a distance of 12 cm from the nozzle are $4 \times 10^{15}/\mathrm{cm}^3$ electron density, 10 eV electron temperature and 102 km s^{-1} ejection velocity (see, in Qi *et al.* 2021). Figure 8(*c*) shows the collision characteristics of the two plasma jets. It is evident that the light intensity increases and is greater than that of the FRC plasma following the plasma jets merging, and the maintenance time is around 8 μs. Compared with the counter-helicity spheromaks merging, the plasma jets merging has stronger light intensity but shorter confinement time. We ascribe this phenomenon to the opposing toroidal magnetic fields. The toroidal magnetic fields of the plasma jets annihilate each other during the collision, the merged plasma has no magnetic field confinement, and its maintenance time is therefore expected to be reduced.

The corresponding time-integrated radiation image of the plasma jets merging is shown in figure 9. It can be seen that the shape of the plasma formed by the merging of jets is divergent, and the luminous intensity is bright at the core and diffused around. For a single

https://doi.org/10.1017/S0022377824000813 Published online by Cambridge University Press

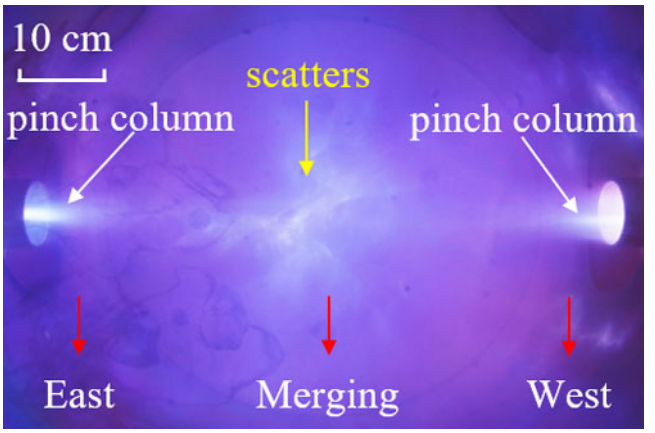

FIGURE 9. Radiation image of two plasma jets merging for a 13 kV shot and an exposure of 1 s. View perpendicular to the gun axis.

plasma jet, there is a pinch effect in the formation process, with a bright plasma column approximately $1 \sim 2$ cm in diameter in the centre, surrounded by a diffuse plasma plume. In the head-on collision of two plasma jets, it is generally assumed that the internal toroidal magnetic fields rapidly annihilate each other during the collision. The merger will begin with collisionless interpenetration and then transitions to collisional stagnation, which is typical of supersonic plasma jet collisions (Moser & Hsu 2015). The overall profile of the merging body is scattering like current filaments. The results suggest that the merged plasma has a higher-energy centre than the FRC plasma, spreads from the centre to all sides under the action of thermal expansion and the thermal expansion is extremely uneven, so there is no clear profile overall.

A schematic diagram of the counter-helicity spheromak merger and plasma jet merger processes is provided to qualitatively account for the plasma morphology in the experiment, as shown in figure 10. The magnetic field configuration is an important factor affecting plasma morphology. For the formation of the spheromak, the toroidal magnetic field in the ejected spheromak retains the accelerating field configuration due to the 'frozen-in-field-line' effects, whereas the stretching and reconnection of the bias magnetic lines is the source of the poloidal magnetic field, in which the toroidal magnetic field nests with the poloidal magnetic field (Loewenhardt, Yee & Bellan 1995). For the formation of the plasma jet, only the toroidal magnetic field is retained inside. In counter-helicity spheromaks merging, two spheromaks with opposite toroidal magnetic flux merge together, and then an FRC with no toroidal magnetic flux is generated. Since the FRC plasma mainly has only a poloidal magnetic field, the plasma pressure at the null must be equal to the radial pressure exerted by the external field in equilibrium

$$B_e^2 = 2\mu_0 nk(T_i + T_e). \tag{3.1}$$

where B_e is the external magnetic field of the FRC, n is the number density of particles, T_i and T_e represent the ion and electron temperature, respectively. In plasma jet mergers, the toroidal magnetic fields of the two jets are annihilated. The merged plasma without magnetic field constraint, expands around under the plasma pressure, so the morphology is indistinct.

https://doi.org/10.1017/S0022377824000813 Published online by Cambridge University Press

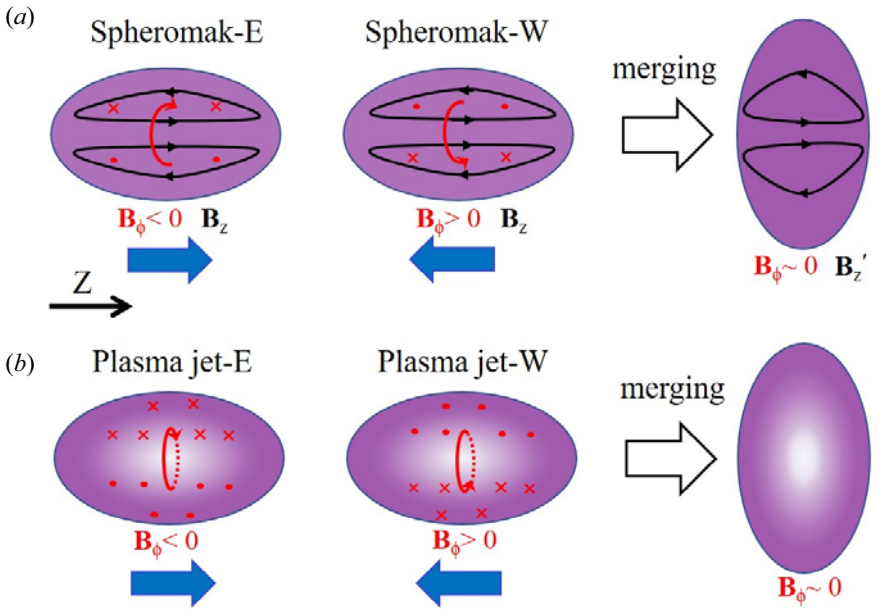

FIGURE 10. Schematic diagrams of (*a*) counter-helicity spheromaks merging and (*b*) plasma jets merging.

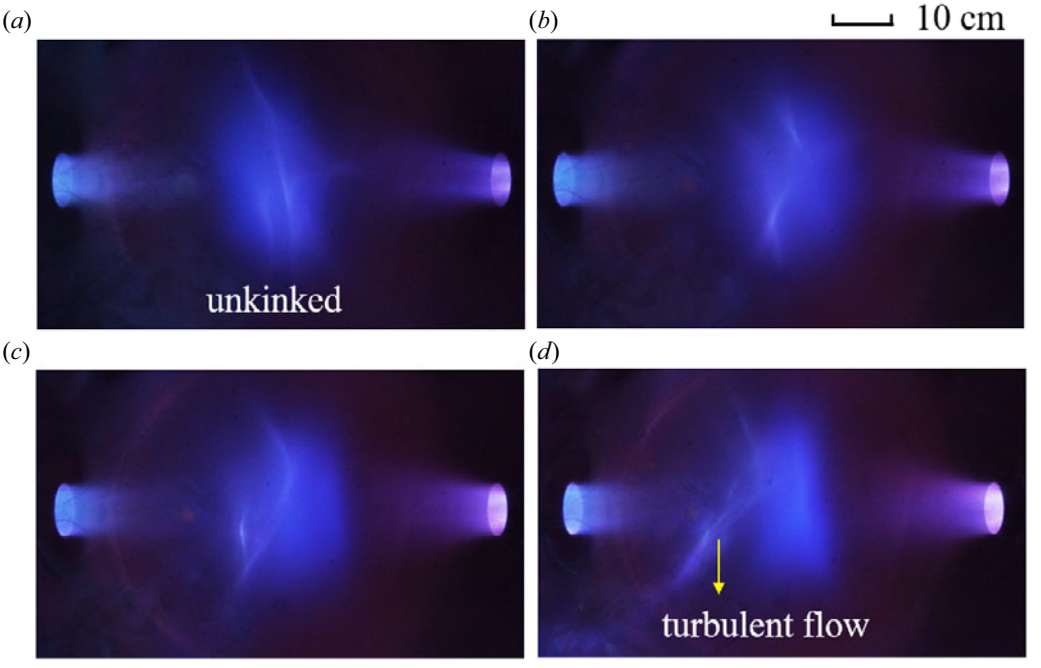

FIGURE 11. Radiation images for counter-helicity spheromaks merging with the gas-puffed mass of 0.46 mg at different discharge voltages (*a*) 12 kV, (*b*) 13 kV, (*c*) 14 kV and (*d*) 15 kV. The exposure time of the images is 1 s.

https://doi.org/10.1017/S0022377824000813 Published online by Cambridge University Press

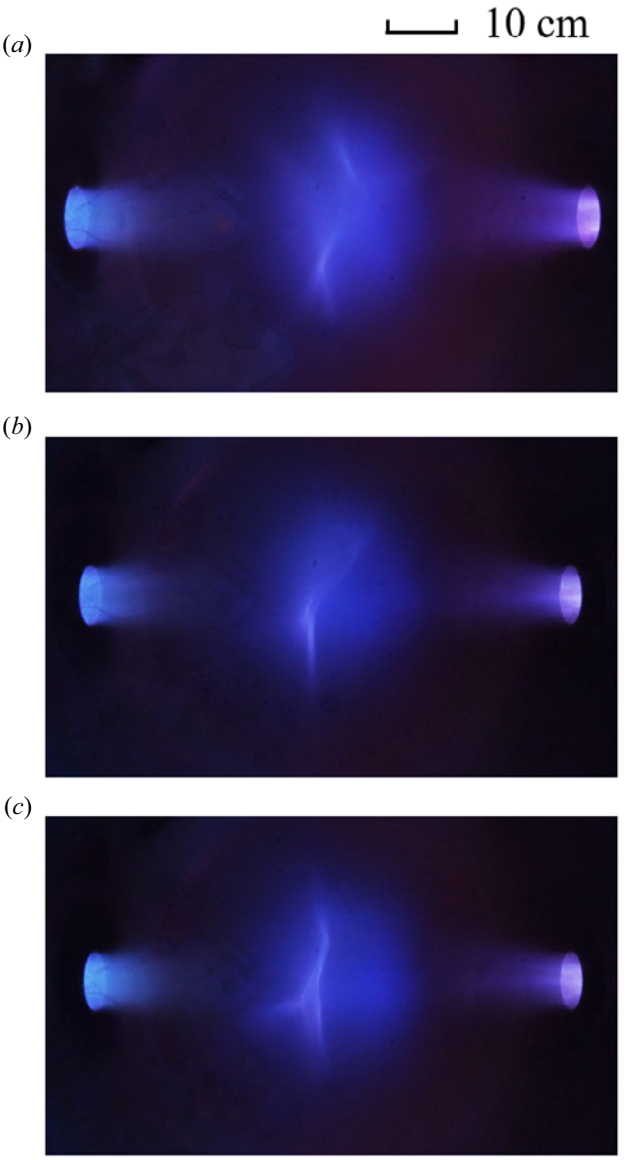

FIGURE 12. Radiation images for counter-helicity spheromaks merging with the discharge voltage of 13 kV at different gas-puffed masses (*a*) 0.46 mg, (*b*) 0.54 mg and (*c*) 0.61 mg. The exposure time of the images is 1 s.

3.3. *Effect of discharge parameters on counter-helicity spheromaks merging*

Operating parameters are critical for the formation and optimization of counter-helicity spheromaks merging. Under a fixed bias magnetic flux (2.7 mWb), the effects of different discharge voltages and gas-puffed masses on the counter-helicity spheromaks merging are investigated. Figure 11 shows the time-integrated radiation images of counter-helicity spheromaks merging at a fixed gas-puffed mass of 0.46 mg and discharge voltages of 12, 13, 14 and 15 kV. It is obvious that, with the increase of the discharge voltage, the bright merging surface deviates from the midplane. At 11 kV, only collision and

https://doi.org/10.1017/S0022377824000813 Published online by Cambridge University Press

compression occurred between the counter-helicity spheromak, and no kink occurred in the midplane, while bright filaments were found to detach from the merged body at 15 kV. These phenomena are considered to be directly related to the plasma flow caused by the possibly complex magnetic topology. Considering the coaxial gun acceleration process, the momentum of the plasma in the gun is the integral of the Lorentz force with time $P = \frac{1}{2}L' \int I^2 \, \mathrm{d}t$ (I is the discharge current, L' is the inductance gradient). We expect that the kinetic energy of the spheromak plasma increases with the storage power supply voltage, possibly increasing the rate of thermalization upon collision. The higher plasma pressure in the FRC compared with the magnetic pressure causes the balance between the plasma pressure and the magnetic pressure to be disrupted. Since the evolution of the spheromaks are not limited by the size of the chamber or the external magnetic field, the radially expanding merged plasma has the possibility to shunt current into the vacuum chamber walls. As a result, the magnetic field structure of the FRC might be damaged, and the internal plasma flow might therefore tend to be turbulent, allowing current filaments to flow to the vacuum walls.

Figure 12 shows the time-integrated radiation images of counter-helicity spheromaks merging at a fixed discharge voltage of 13 kV and gas-puffed masses of 0.46, 0.54 and 0.61 mg. It can be seen that the kink characteristics of the merged surface show little change with the increase of the gas-puffed mass, but there is a slight difference in the morphology of the merged body. When the gas-puffed mass is increased, the axial size of the merged body increases, while the radial size decreases. The ratios of radial to axial lengths are 1.36, 1.17 and 1.01 and the whole body tends to be a sphere. We expect that the plasma momentum is independent of the gas-puffed mass because the larger gas-puffed mass results in a lower plasma velocity, but the total momentum remains the same. Therefore, under the same discharge voltage, the gas-puffed mass has little effect on the momentum gain of the plasma from the capacitor bank or the plasma pressure after merger, which may have no impact on the magnetic field structure of the FRC plasma. However, increasing the gas-puffed mass results in a slower ejection velocity for spheromak, which weakens the compression effect during the merger.

4. Conclusions

In this paper, the formation and evolution of counter-helicity spheromaks merging by magnetized coaxial plasma gun are experimentally investigated. At fixed initial conditions (charging voltage, gas puff), the time-dependent photodiode signals and plasma radiation images of counter-helicity spheromaks merging and plasma jets merging are compared and analysed. From the data, the ejection characteristics of the spheromak or jet are obtained, and the dynamics of the magnetic field topology is inferred from consistent photodiode signals and radiation images. The results suggest that what are identified as possible collisional heating and magnetic reconnection events occur during the merging of the high-speed spheromaks, which causes an increase of light intensity ascribed to a quickly rising plasma pressure. In addition, the FRC plasma formed by the unconfined counter-helicity spheromaks merging is only confined by the poloidal magnetic field, which shows clear luminous profiles and twisted bright filaments near the merger region. As for the plasma jets merging, since the toroidal magnetic fields of the plasma jets are annihilated during the collision process, the merged plasma has no magnetic field confinement, hence its lifetime must be shortened. The light intensity of the merged body diverges from the centre to the edge, and the whole body has no obvious contour.

The effects of different operating parameters on the counter-helicity spheromak merger characteristics are investigated, and the qualitative dynamics of the FRC depends on the balance between thermal and magnetic pressures. It is speculated that the increase of

https://doi.org/10.1017/S0022377824000813 Published online by Cambridge University Press

discharge voltage increases the momentum of the spheromak, which leads to the break of the equilibrium between the merged plasma pressure and the magnetic pressure, the internal magnetic field structure is unstable and the plasma flow tends to be turbulent. However, when the gas-filled mass increases, the FRC plasma pressure and its internal magnetic field structure may be relatively unaffected, as the spheromaks' momentum is expected to be unaffected by the gas-fill mass. It only weakens the compression effect during the merger process, resulting in an increase in the axial size of the merged body and a decrease in the radial size, and the whole is close to a spherical shape.

Counter-helicity spheromaks merging is expected to yield a stable, long-lifetime FRC magnetized target. In this experiment, the FRC plasma is formed by the unconfined counter-helicity spheromaks merging, and the absence of an external magnetic field confinement allows for a better understanding of the physical mechanisms governing FRC's own confinement and maintenance. The detailed experimental results reveal the formation and evolution of the counter-helicity spheromaks merging, as well as their dependence on different discharge parameters, and hopefully provide a reference for future experimental optimization design.

Acknowledgements

Editor Cary Forest thanks the referees for their advice in evaluating this paper.

Funding

This work was supported by National Key R&D Program of China Grant Nos. 2017YFE0301804 and 2017YFE0301206, National Natural Science Foundation of China Grant No. 51807020 and Tianyou Youth Talent Lift Program of Lanzhou Jiaotong University: 4th Batch.

Declaration of interests

The author reports no conflict of interest.

Data availability

The authors confirm that all of the data and codes used in this study are available from the corresponding author upon reasonable request.

REFERENCES

Belova, E.V., Davidso, R.C., Ji, H., Yamada, M., Cothra, C.D., Brown, M.R. & Schaffer, W. 2006 Numerical study of the formation, ion spin-up and nonlinear stability properties of field-reversed configurations. *Nucl. Fusion* **46**, 162.

Brown, M.R. & Bellan, P.M. 1992 Efficiency and scaling of current drive and refuelling by spheromak injection into a tokamak. *Nucl. Fusion* **32**, 1125.

Brown, M.R., Cothran, C.D., Fung, J., Chang, M., Horwitz, J., Schaffer, M.J., Leuer, J. & Belova, E.V. 2006 Dipole trapped spheromak in a prolate flux conserver. *Phys. Plasmas* **13**, 1717.

Brown, M.R., Cothran, C.D., Landreman, M., Schlossberg, D., Matthaeus, W.H., Qin, G., Lukin, V.S. & Gray, T. 2002 Energetic particles from three-dimensional magnetic reconnection events in the Swarthmore Spheromak Experiment. *Phys. Plasmas* **9**, 2077.

Byvank, T., Endrizzi, D.A., Forest, C.B., Langendorf, S.J., Mccollam, K.J. & Hsu, S.C. 2021 Formation of transient high-β plasmas in a magnetized, weakly collisional regime. *J. Plasma Phys*. **87**, 905870202.

Cothran, C.D., Brown, M.R., Gray, T., Schaffer, M.J. & Lukin, V.S. 2010 Observation of a nonaxisymmetric magnetohydrodynamic self-organized state. *Phys. Plasmas* **17**, 055705.

https://doi.org/10.1017/S0022377824000813 Published online by Cambridge University Press

COTHRAN, C.D., FALK, A., FEFFERMAN, A., LANDREMAN, M., BROWN, M.R. & SCHAFFER, M.J. 2003 Spheromak merging and field reversed configuration formation at the Swarthmore Spheromak Experiment. *Phys. Plasmas* **10**, 1748.

FURTH, H.P. 1981 Compact torus. *J. Vac. Sci. Technol*. **18**, 1073.

GEDDES, C.G.R., KORNACK, T.W. & BROWN, M.R. 1998 Scaling studies of spheromak formation and equilibrium. *Phys. Plasmas* **5**, 1027.

GERHARDT, S.P., BELOVA, E.V., YAMADA, M., JI, H. & REN, Y. 2008 Field-reversed configuration formation scheme utilizing a spheromak and solenoid induction. *Phys. Plasmas* **15**, 032503.

GRAY, T., LUKIN, V.S., BROWN, M.R. & COTHRAN, C.D. 2010 Three-dimensional reconnection and relaxation of merging spheromak plasmas. *Phys. Plasmas* **17**, 102106.

HOFFMAN, A.L., GUO, H.Y., MILLERA, K.E. & MILROY, R.D. 2006 Principal physics of rotating magnetic-field current drive of field reversed configurations. *Phys. Plasmas* **13**, 012507.

HORIUCHI, R., MORITAKA, T.A. & USAMI, S. 2018 PIC simulation study of merging processes of two spheromak-like plasmoids. *Plasma Fusion Res*. **13**, 3403035.

HSU, S.C. & BELLAN, P.M. 2005 On the jets, kinks, and spheromaks formed by a planar magnetized coaxial gun. *Phys. Plasmas* **12**, 032103.

JANOS, A., HART, G.W., NAM, C.H. & YAMADA, M. 1985 Global magnetic fluctuations in spheromak plasmas and relaxation toward a minimum-energy state. *Phys. Fluids* **28**, 3667.

JARBOE, T.R. 1994 Review of spheromak research. *Plasma Phys. Control. Fusion* **36**, 945–990.

JARBOE, T.R. 2005 The spheromak confinement device. *Phys. Plasmas* **12**, 058103.

KAMINOU, Y., GUO, X., INOMOT, M., ONO, Y. & HORIUCHI, R. 2017 Numerical study of Hall effects on counter-helicity spheromak merging by two-dimensional Hall-MHD simulations. *Phys. Plasmas* **24**, 032508.

KAWAMORI, E. & ONO, Y. 2005 Effect of ion skin depth on relaxation of merging spheromaks to a field-reversed configuration. *Phys. Rev. Lett*. **95**, 085003.

KOBAYASHI, D., ASAI, T., TAKAHASHI, T., TATSUMI, A., SAHARA, N., WATANABE, T., HARASHIMA, D., GOTA, H. & WATANABE, T. 2021 Energy flow in the super alfvénic/sonic collisional merging process of field-reversed configurations. *Plasma Fusion Res*. **16**, 2402050.

KORNACK, T.W., SOLLINS, P.K. & BROWN, M.R. 1998 Experimental observation of correlated magnetic reconnection and Alfvénic ion jets. *Phys. Rev. E* **58**, R36.

LOEWENHARDT, P.K., YEE, J. & BELLAN, P.M. 1995 Performance characterization of the Caltech corn act torus injector. *Rev. Sci. Instrum*. **66**, 1050.

LUKIN, V.S., QIN, G., MATTHAEUS, W.H. & BROWN, M.R. 2001 Numerical modeling of magnetohydrodynamic activity in the Swarthmore Spheromak Experiment. *Phys. Plasmas* **8**, 1600.

MAKWANA, K.D., KEPPENS, R. & LAPENTA, G. 2018 Study of magnetic reconnection in large-scale magnetic island coalescence via spatially coupled MHD and PIC simulations. *Phys. Plasmas* **25**, 082904.

MATSUMOTO, T., SEKIGUCHI, J., ASAI, T., GOTA, H., GARATE, E., ALLFREY, I., VALENTINE, T., MOREHOUSE, M., ROCHE, T., KINLEY, J., AEFSKY, S., CORDERO, M., WAGGONER, W., BINDERBAUER, M. & TAJIMA, T. 2016 Development of a magnetized coaxial plasma gun for compact toroid injection into the C-2 field-reversed configuration device. *Rev. Sci. Instrum*. **87**, 053512.

MOSER, A.L. & HSU, S.C. 2015 Experimental characterization of a transition from collisionless to collisional interaction between head-on-merging supersonic plasma jets. *Phys. Plasmas* **22**, 055707.

NAGATA, M., OGAWA, H., YATSU, S., FUKUMOTO, N., KAWASHIMA, H., TSUZUKI, K., NISHINO, N., UYAMA, T., KASHIWA, Y., SHIBATA, T., KUSAMA, Y. 2005 Experimental studies of the dynamics of compact toroid injected into the JFT-2M tokamak. *Nucl. Fusion* **45**, 1056.

NISHIDA, K., HORIUCHI, R. & ONO, Y. 2019 Analysis of energy conversion during co- and counter-helicity spheromak merging by particle-in-cell simulation. *Plasma Fusion Res*. **14**, 3401145.

ONO, Y., INOMOTO, M., UEDA, Y., MATSUYAMA, T. & OKAZAKI, T. 1999 New relaxation of merging spheromaks to a field reversed configuration. *Nucl. Fusion* **39**, 2001.

ONO, Y., YAMADA, M. & AKAO, T. 1996 Ion acceleration and direct ion heating in three-component magnetic reconnection. *Phys. Rev. Lett*. **76**, 3328.

PARKS, P.B. 1988 Refueling tokamaks by injection of compact toroids. *Phys. Rev. Lett*. **61**, 1364.

PIERCE, W.F., MAQUEDA, R.J., BROOKS, R.D. & FARENGO, R. 1993 Initial results from parallel coil operation of the Coaxial Slow Source field reversed configuration device. *Nucl. Fusion* **33**, 117.

PIETRZYK, Z.A., VLASES, G.C., BROOKS, R.D., HAHN, K.D. & RAMAN, R. 1987 Initial results from the coaxial slow source FRC device. *Nucl. Fusion* **27**, 1478.

QI, L.W., SONG, J., ZHAO, C.X., BAI, X.D., ZHAO, F.T., YAN, H.J., REN, C.S. & WANG, D.Z. 2020 Research on an unconfined spheromak and its current path in a magnetized coaxial plasma gun. *Phys. Plasmas* **27**, 122506.

QI, L.W., SONG, J., ZHAO, F.T., ZHAO, C.X., YAN, H.J. & WANG, D.Z. 2021 Effects of bias magnetic field on plasma ejection and dynamic characteristics of a coaxial gun operated in gas-puffed mode. *Plasma Phys. Control. Fusion* **63**, 115008.

STANIC, M., CASSIBRY, J.T. & ADAMS, R.B. 2013 Project Icarus: analysis of plasma jet driven magneto-inertial fusion as potential primary propulsion driver for the Icarus probe. *Acta Astronautica* **86**, 47.

STEINHAUER, L.C. 2011 Review of field-reversed configurations. *Phys. Plasmas* **18**, 070501.

VYAS, A.C. & CASSIBRY, J.T. 2020 *AIAA propulsion and energy* 2020 Forum.

YAMADA, M., ONO, Y., HAYAKAWA, A., KATSURAI, M. & PERKINS, F.W. 1990 Magnetic reconnection of plasma toroids with cohelicity and counterhelicity. *Phys. Rev. Lett*. **65**, 721.

YAMADA, M., YOO, J., JARA-ALMONTE, J., JI, H., KULSRUD, R.M. & MYERS, C.E. 2014 Conversion of magnetic energy in the magnetic reconnection layer of a laboratory plasma. *Nat. Commun*. **5**, 4774.

YOO, J., YAMADA, M., JI, H. & MYERS, C.E. 2013 Observation of ion acceleration and heating during collisionless magnetic reconnection in a laboratory plasma. *Phys. Rev. Lett*. **110**, 215007.